Supporting Information: Strong Light-Matter Coupling in Pentacene Thin Films on Plasmonic Arrays

Christoph P. Theurer[a], Florian Laible[a], Jia Tang[a], Katharina Broch[a,b], Monika Fleischer[*a,b], and Frank Schreiber[*a,b]

[a] Institut für Angewandte Physik, Universität Tübingen, Auf der Morgenstelle 10, 72076 Tübingen, Germany.

[b] Center for Light-Matter Interactions, Sensors & Analytics (LISA$^+$), Universität Tübingen, Auf der Morgenstelle 15, 72076 Tübingen, Germany.

[*] E-mail: monika.fleischer@uni-tuebingen.de, frank.schreiber@uni-tuebingen.de

1 Nanoantenna fabrication

The nanoantennas were fabricated by electron beam lithography. As positive electron-beam resist a ∼120 nm thick poly(methyl methacrylate) (PMMA) (DuPont, average chain length 4041 monomers) layer was spin-coated (6 s at 2600 rpm, followed by 60 s at 5000 rpm) on cleaned coverslips (n=1.51) as substrates. On top, a thin layer of a conducting polymer (AR-PC 5090.02 (Electra 92) from Allresist) was spun (40 s at 4000 rpm) to obtain the desired conductivity for electron-beam lithography. The lithography was performed on a FEI XL30 scanning electron microscope (SEM) equipped with a Xenos XPA 2 pattern generator controlled by the ECP software. After the exposure, the Electra 92 was removed by placing the sample for 30 s in deionized water. The following development of the sample was carried out for 70 s in a mixture of isopropanol and methyl isobutyl ketone in a 3:1 ratio. Afterward, the sample was dried in a nitrogen flow and placed in a Pfeiffer Vacuum PLS 570 evaporator for metal deposition. First, a ∼2 nm thick titanium layer was deposited by electron-beam physical vapor deposition to increase the adhesion of the silver particles to the substrate. Subsequently, a 35 nm silver layer was applied via thermal evaporation. The deposition rates were ∼1.5 nm/min and ∼1 nm/min for Ti and Ag, respectively, monitored by a thickness-calibrated quartz crystal microbalance. The error in the silver thickness is estimated to ±10 % from profilometer measurements on reference samples.

As mentioned in the main text, besides the arrays of nanorods that form the main topic of this work, additional arrays with different particle sizes and shapes, as well as different lattice parameters and geometries, were produced. The particle sizes, standard deviations and lattice parameters of the nanorods are included in the main text.

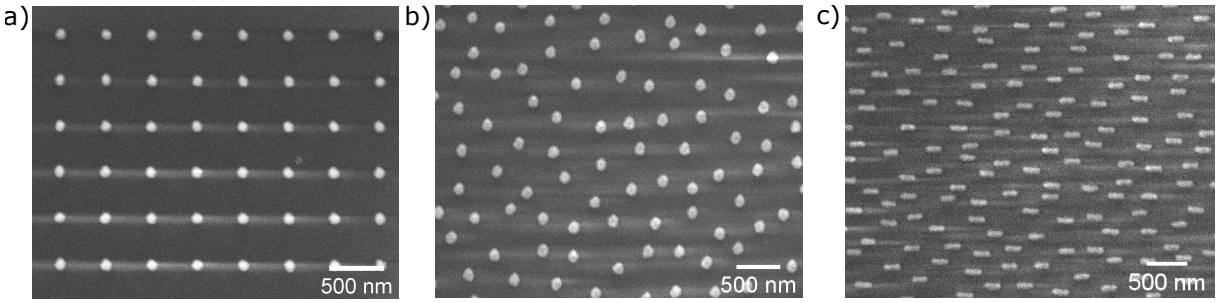

Figure S1: SEM images of exemplary samples of silver nanoparticles on glass, with a covering layer of 10 nm Al_2O_3 over the entire surface. a) A square array of discs, b) randomly distributed discs, and c) randomly distributed rods are shown.

Ordered square nanodisc arrays were produced with lattice constants of $a = 415\,\text{nm}$ and $a = 410\,\text{nm}$, and disc diameters of $d = 85\,\text{nm}$ and $d = 100\,\text{nm}$, respectively, for comparison reasons. While they show less strongly pronounced features than the nanorod arrays, the square arrays of discs possess a higher symmetry than the rectangular arrays of rods, which allows to obtain similar spectra under polarized and unpolarized excitation [1]. This might be of interest for further investigations and applications.

Additionally, to remove the influence of the SLR and to analyze the resulting coupling, samples with randomly distributed discs or rods were fabricated that do not exhibit collective modes. The diameter of the discs was $d = 110\,\text{nm}$. The rods were all oriented with their long axis along the x-direction and the dimensions were $w = 85\,\text{nm}$ and $s = 225\,\text{nm}$.

Finally, also samples with much larger discs, namely with a diameter of $d = 180\,\text{nm}$, were fabricated. This large diameter was chosen to obtain low-energy LSPRs that are non-resonant to the PEN transitions. Hence, the influence of the LSPR coupling to the PEN transitions is also removed in these samples. This allows to compare the undisturbed spectra of the PEN film on and beside the array which yields information about the molecular orientation. Exemplary SEM images of samples of discs and rods, with regular or random distribution, are shown in Figure S1.

2 Electric field simulation of rod arrays

The rod arrays are simulated with the finite element method (FEM) simulation software Comsol Multiphysics. The simulation model contains one unit cell of a grating consisting of a silver rod (width: 85 nm, length 200 nm, and height 40 nm) which is covered by a 10 nm thick aluminum oxide layer. Underneath the rod, the material is glass, and the upper half space contains a 130 nm thick layer of polystyrene (n = 1.59; k = 0). The rest of the model is air. Periodic boundary conditions are used to simulate an infinite periodic array of the nanoparticles. The rectangular footprint of the unit cell defines the grating constants in the x- and y-direction (here $a_x = 190\,\text{nm}$; $a_y = 415\,\text{nm}$).

The model is excited by a plane electromagnetic wave that enters the model from a port on the top and leaves it through a port on the bottom. The electric field is oriented along the short axis of the rod and the k-vector is perpendicular to the substrate. The wavelength is swept from 400 nm to 750 nm (3.1 eV to 1.65 eV) in 5 nm steps. The difference in power between the two ports for each wavelength gives the absorbed power (extinction)

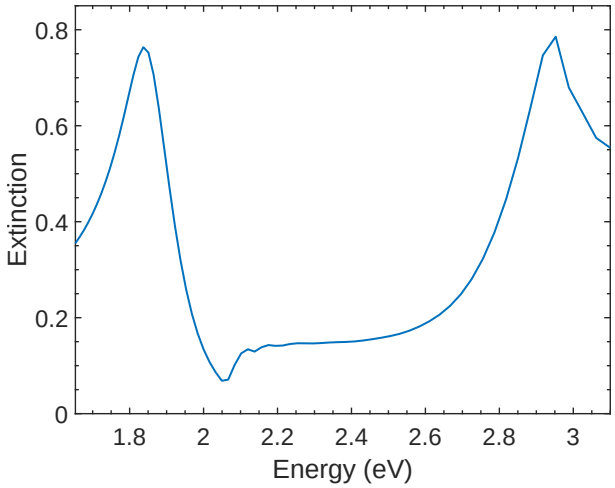

Figure S2: Simulated extinction spectrum, showing the SLR around 1.84 eV and the LSPR around 2.95 eV.

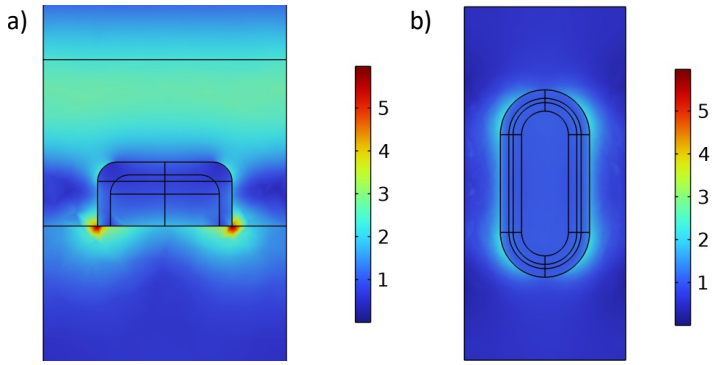

Figure S3: Electric field distribution at 2.952 eV excitation energy. a) side view, b) top view.

spectrum shown in Figure S2. This spectrum closely resembles the experimentally obtained extinction spectra of the rod arrays covered by polystyrene, demonstrating the successful simulation of the experimental conditions. The peak slightly below 3 eV can be attributed to the LSPR of the single particles. This is deduced from the electric field distribution at 2.952 eV, shown in Figure S3, which exhibits an electric field enhancement localized close to the particle edges. All shown field distributions are normalized to the incident field strength and color-coded accordingly. The peak around 1.837 eV in Figure S2 is caused by the SLR of the grating, inferable from the electric field distribution at this energy, presented in Figure S4. At this SLR energy, the electric field distribution shows an enhanced field in the volume between the particles in the x-direction. Additionally, an enhanced field is obtained between the rows of nanorods in y-direction (see Fig. S4b), thus delocalized away from the particles, which is a clear sign for a SLR. The maximal field enhancement in the top view is 5.4. The mean electric field enhancement in the volumes between the nanorods in x-direction is $\gtrsim 3$. The regions of high electric field enhancement constitute the mode volume where strong interaction with the pentacene molecules takes place. Furthermore, a fraction of the volume that exhibits a strongly enhanced field is located inside the glass substrate (see e.g. Figure S4a), which can therefore not be occupied by PEN molecules and thus does not contribute to the light-matter coupling.

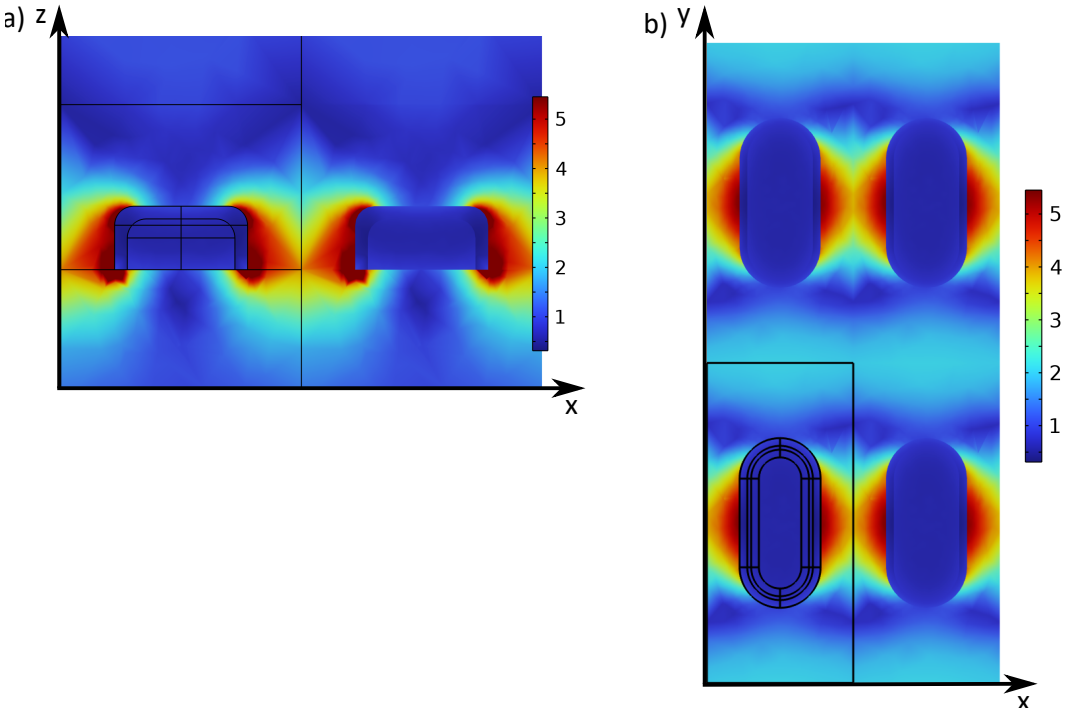

Figure S4: Electric field distribution at 1.837 eV excitation energy. a) side view of two unit cells (the original unit cell has black outlines; the second cell is a copy). b) Top view of four unit cells (the original unit cell has black outlines; the other cells are copies).

3 Additional array spectra

In Figure S5 and Figure S6, additional extinction spectra of further rod arrays with slightly different average rod dimensions are shown, covered by PS and PEN, respectively. The extinction spectra of these arrays are very similar to the ones shown in the main text, illustrating the reproducibility and tolerance to minor changes in the dimensions.

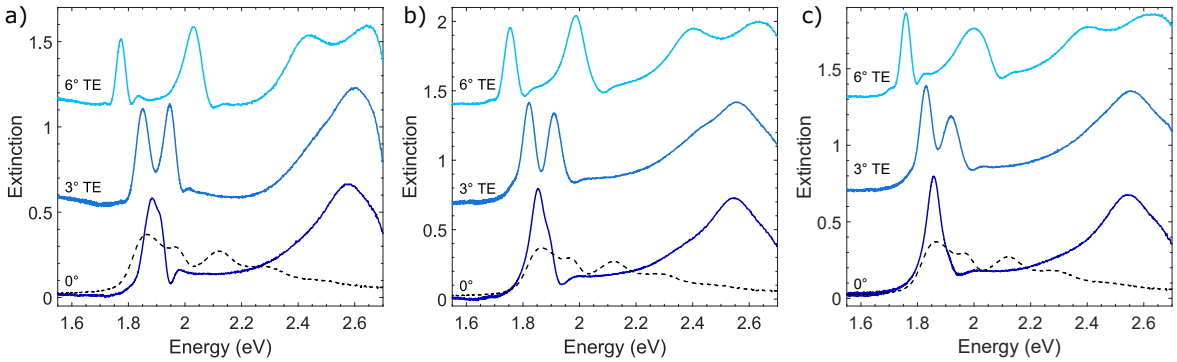

Figure S5: Extinction spectra of plasmonic rod arrays covered by a polystyrene reference film. The dimensions of the lattices are $a_x = 415$ nm and $a_y = 190\,\mathrm{nm}$ for all arrays, while the rod dimensions are: a) $220\,\mathrm{x}\,90\,\mathrm{nm}^2$, b) $220\,\mathrm{x}\,95\,\mathrm{nm}^2$ and c) $215\,\mathrm{x}\,95\,\mathrm{nm}^2$. The spectra taken under $\theta = 3°$ and $\theta = 6°$ are vertically offset for clarity. The black dashed spectrum is the extinction spectrum of a PEN thin film for peak position comparison.

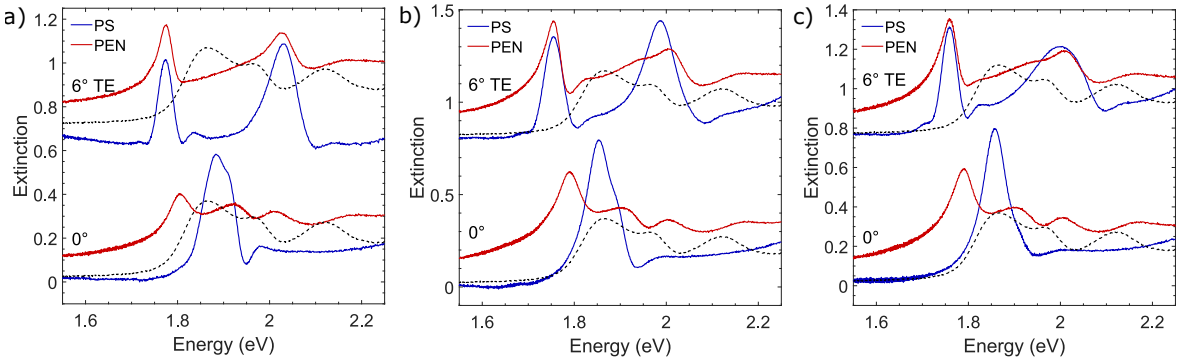

Figure S6: Extinction spectra of the same plasmonic rod arrays as in Figure S5, covered with a 50 nm PEN film (red) and PS for reference (blue). The dimensions of the lattices for all arrays are $a_x = 415$ nm and $a_y = 190\,\mathrm{nm}$, while the rod dimensions are: a) $220\,\mathrm{x}\,90\,\mathrm{nm}^2$, b) $220\,\mathrm{x}\,95\,\mathrm{nm}^2$ and c) $215\,\mathrm{x}\,95\,\mathrm{nm}^2$. The spectra taken under $\theta = 6°$ are vertically offset for clarity. The black dashed spectrum is the extinction spectrum of the PEN thin film recorded beside the array for peak position comparison.

In Figure S7 and Figure S8, similarly the extinction spectra of square arrays consisting of discs are shown, again covered by PS and PEN, respectively. From a comparison of the spectra in Figure S7 to the ones in Figure S5, it is apparent that the maximum extinction of the SLRs is reduced in the arrays of discs and that they are broadened, especially under non-normal illumination. Still, SLRs are also realized in the disc array spectra at the energy of E^+. Figure S8 shows that these SLRs also couple to the PEN transitions, but the polariton bands are less clearly pronounced and the spectra under $\theta = 6°$ are more difficult to interpret.

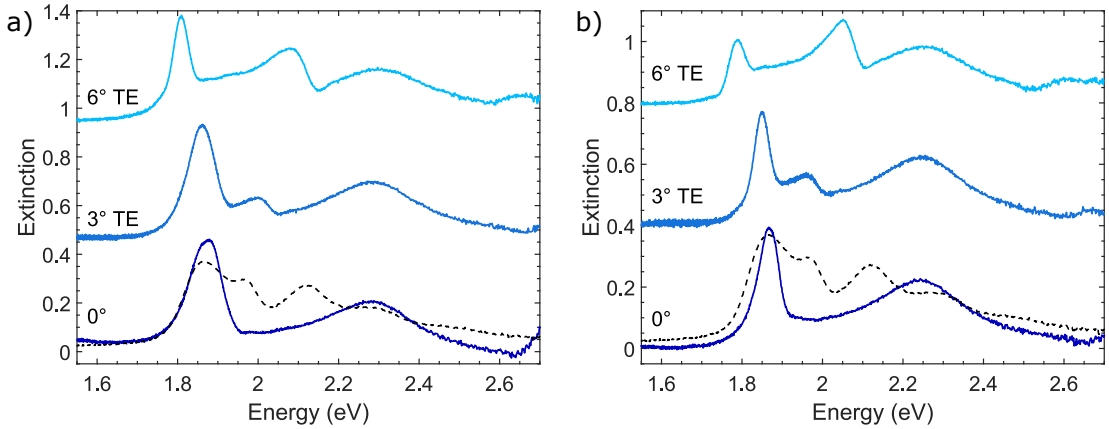

Figure S7: Extinction spectra of plasmonic disc arrays covered by a polystyrene reference film. The dimensions are: a) $a_x = a_y = 410$ nm and $d = 100\,\text{nm}$, and b) $a_x = a_y = 415$ nm and $d = 85\,\text{nm}$. The spectra taken under $\theta = 3°$ and $\theta = 6°$ are vertically offset for clarity. The black dashed spectrum is the extinction spectrum of a PEN thin film for peak position comparison.

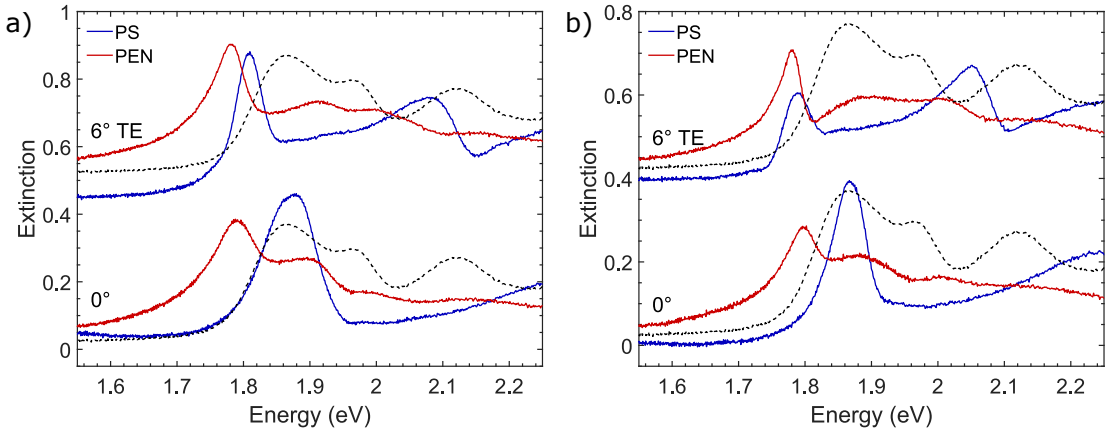

Figure S8: Extinction spectra of the same plasmonic disc arrays as in Figure S7, covered with a 50 nm PEN film (red) and PS for reference (blue). The dimensions are: a) $a_x = a_y = 410$ nm and $d = 100\,\text{nm}$ and b) $a_x = a_y = 415$ nm and $d = 85\,\text{nm}$. The spectra taken under $\theta = 6°$ are vertically offset for clarity. The black dashed spectrum is the extinction spectrum of the PEN thin film recorded beside the array for peak position comparison.

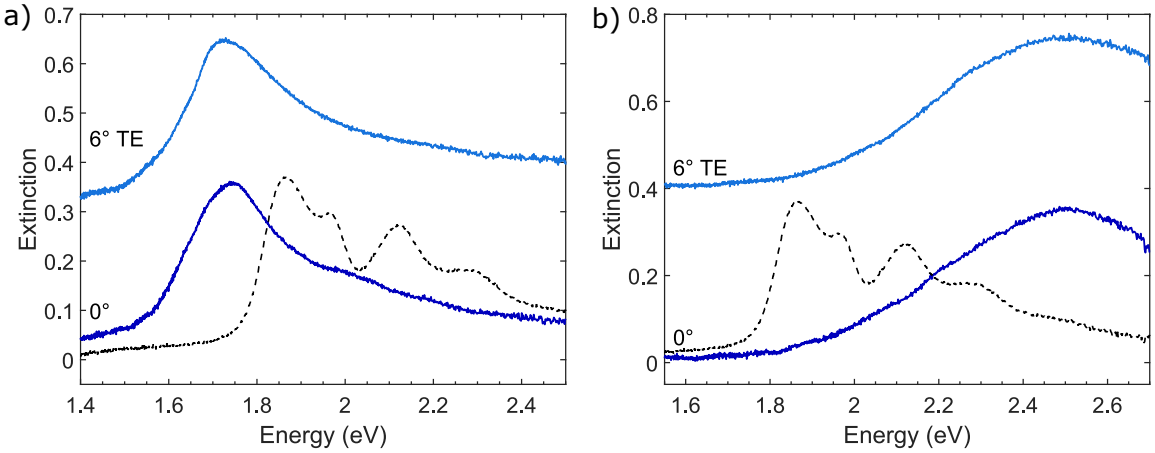

Figure S9: Extinction spectra of randomly distributed a) discs with $d = 110\,\text{nm}$ and b) rods with $w = 85\,\text{nm}$ and $s = 225\,\text{nm}$, covered by a polystyrene reference layer. The rods were still oriented with their long axis along x and the polarization of the light was along y. The black dashed spectrum is the extinction spectrum of a PEN thin film for peak position comparison.

In Figure S9, extinction spectra of samples with randomly distributed a) discs, or b) rods, covered by a reference PS layer, are shown (see Figure S1 for exemplary SEM images). They clearly show only LSPRs of the single particles, while SLRs are absent due to the lack of long-range order. As expected, these spectra are insensitive to small rotations which introduce a wave vector component parallel to the substrate. The discs with diameter d =110 nm show an extinction maximum at ∼1.75 eV, and the rods with dimensions of s =225 nm and w = 85 nm one at ∼2.5 eV for excitation along their short axis. These single particle resonances are hence non-resonant to the two DCs in the PEN extinction spectrum. Nevertheless, the spectra show some changes when the PS layer is replaced by a PEN thin film (cf. Figure S10). For the discs the extinction maximum is shifted to ∼1.67 eV and a second maximum around the energy of E^+ is visible. This second peak can be explained by neat PEN absorption which was not entirely subtracted. Generally, several transmission spectra of the PEN film around the arrays were recorded as background, which slightly differ in intensity due to small thickness differences. From these spectra always the one with the smallest intensity was chosen as background to calculate the final extinction spectrum by Equation 1 in the main text. This conservative choice was taken to avoid the possibility of subtracting too much intensity, which could result in an overestimation of the coupling strength. The shift of the main peak, however, indicates a significant near-field coupling of the PEN molecules in close proximity to the silver particles. Since only a small fraction of the PEN molecules can couple to the LSPRs, the signal in the PEN absorption region is only slightly influenced. The spectra of the rods are overall less influenced by the PEN transitions since they are further out of resonance.

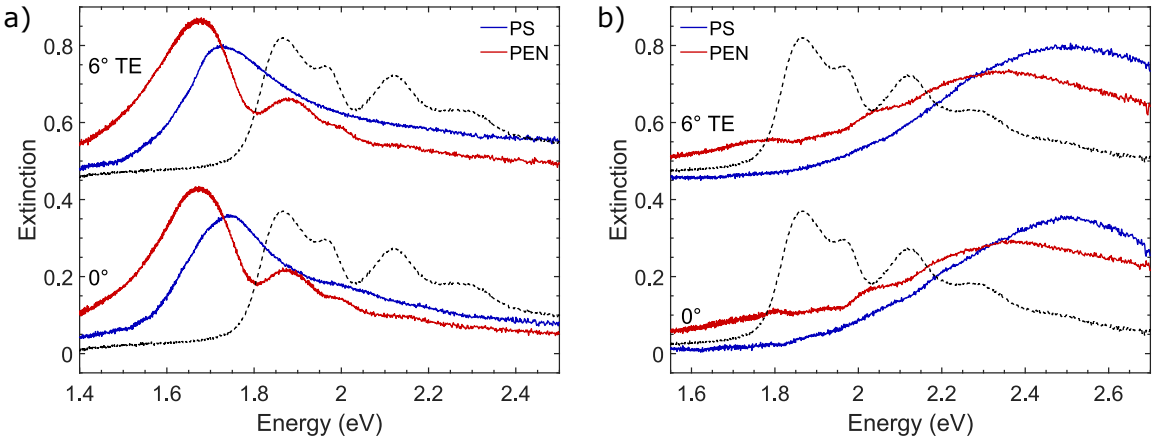

Figure S10: Extinction spectra of the same randomly distributed a) discs with $d = 110\,\text{nm}$ and b) rods with $w = 85\,\text{nm}$ and $s = 225\,\text{nm}$ as in Figure S9, now covered by a 50 nm PEN film. The rods were still oriented with their long axis along x and the polarization of the light was along y. The black dashed spectrum is the extinction spectrum of a PEN thin film beside the array for peak position comparison.

Finally, in Figure S11, the extinction spectrum of a neat PEN film on Al_2O_3 on glass, recorded beside the array, is compared to the extinction spectrum of PEN on an array consisting of discs with a larger diameter ($d = 180\,\text{nm}$). Thus, their LSPR is found at lower energies (around 1.48 eV), non-resonant to the PEN transitions. Therefore, the PEN absorption is not modified by coupling to plasmonic modes of the array. The observed similarity of the spectra in the energy range of the PEN transitions allows to conclude on a similar molecular orientation in both cases, which is almost upright standing for PEN on weakly interacting substrates [2]. If the molecular orientation on the array would be significantly different, the extinction would be decreased, since the transition dipole moments (TDMs) of the two DCs would not be almost perpendicular to the illumination direction anymore. In Figure S12, a simplified illustration of the TDMs of the two DCs in PEN is shown, while further details can be found in Refs. [3, 4].

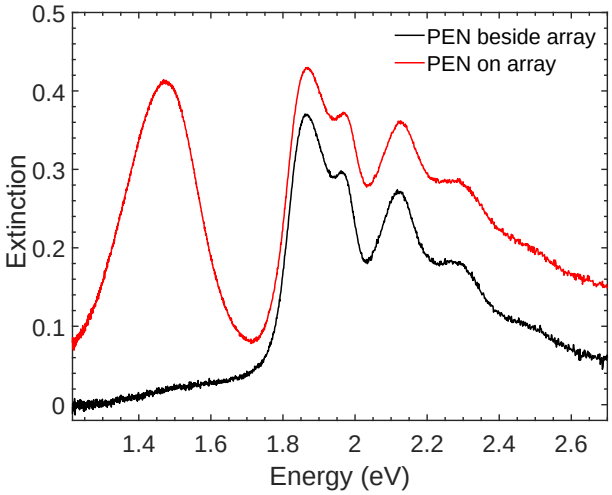

Figure S11: Extinction spectra of a PEN thin film on glass, recorded beside the array (black) and on an array consisting of discs with $d = 180\,\mathrm{nm}$ (red). The strong broad peak around 1.48 eV in the red spectrum is assigned to the LSPR of the particles, but in the energy range of the PEN transitions the spectra are very similar besides the intensity scaling factor due to the light being blocked by the relatively large silver structures.

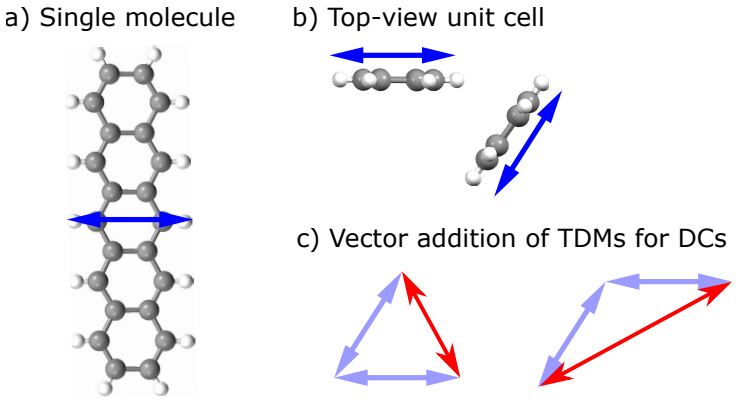

Figure S12: Simplified transition dipole moments (TDMs) in PEN thin films. a) Single, upright-standing PEN molecule with the TDM of the energetically lowest optically allowed transition depicted by a blue arrow. b) Top-view on the herringbone arrangement in the unit cell of the thin film structure of PEN [2]. c) Vector addition of the single-molecule TDMs to obtain the TDMs of the Davydov components (DCs), depicted in red.

References

[1] A. D. Humphrey and W. L. Barnes, Plasmonic surface lattice resonances on arrays of different lattice symmetry, *Phys. Rev. B*, **90**, 075404 (2014).

[2] S. Schiefer, M. Huth, A. Dobrinevski, and B. Nickel, Determination of the crystal structure of substrate-induced pentacene polymorphs in fiber structured thin films, *J. Am. Chem. Soc.*, **129**, 10316 (2007).

[3] C. Cocchi, T. Breuer, G. Witte, and C. Draxl, Polarized absorbance and Davydov splitting in bulk and thin-film pentacene polymorphs, *Phys. Chem. Chem. Phys.*, **20**, 29724 (2018).

[4] N. J. Hestand and F. C. Spano, Expanded theory of H-and J-molecular aggregates: the effects of vibronic coupling and intermolecular charge transfer, *Chem. Rev.*, **118**, 7069 (2018).